

## Phase diagram and $P$ - $V$ - $T$ equation of state of Al-bearing seifertite at lowermost mantle conditions

DENIS ANDRAULT<sup>1,\*</sup>, REIDAR G. TRØNNES<sup>2</sup>, ZUZANA KONÔPKOVÁ<sup>3</sup>, WOLFGANG MORGENROTH<sup>4</sup>,  
HANNS P. LIERMANN<sup>3</sup>, GUILLAUME MORARD<sup>5</sup> AND MOHAMED MEZOUAR<sup>6</sup>

<sup>1</sup>Laboratoire Magmas et Volcans (LMV-OPGC-CNRS), Université B. Pascal, 5 rue Kessler, 63000 Clermont-Ferrand, France

<sup>2</sup>Natural History Museum and Centre for Earth Evolution and Dynamics, University of Oslo, Sem Sealandt vei 24, Blindern, NO-0316 Oslo, Norway

<sup>3</sup>Photone Sciences, Deutsches Elektronen-Synchrotron (DESY), Notkestrasse 85, 22607 Hamburg, Germany

<sup>4</sup>Institut für Geowissenschaften, Goethe University of Frankfurt, Altenhöferallee 1, 60438 Frankfurt am Main, Germany

<sup>5</sup>Institut de Minéralogie, de Physique des Minéraux et de Cosmochimie (IMPMC), 4 place Jussieu, 75005 Paris, France

<sup>6</sup>European Synchrotron Radiation Facility (ESRF), 71 Rue des Martyrs, 38000 Grenoble, France

### ABSTRACT

We investigated the properties of Al-bearing SiO<sub>2</sub> (with 4 or 6 wt% Al<sub>2</sub>O<sub>3</sub>) at pressures and temperatures corresponding to the lowermost mantle, using laser-heated diamond-anvil cell coupled with synchrotron-based in situ X-ray diffraction. The phase transition from CaCl<sub>2</sub>-structured to  $\alpha$ -PbO<sub>2</sub>-structured (seifertite) polymorphs occurs between 113 and 119 GPa at 2500 K. The range of pressure where the two phases coexist is small. There is a slight decrease of the transition pressure with increasing Al-content. We propose a tentative phase diagram reporting the minerals composition as a function of pressure in the SiO<sub>2</sub>-Al<sub>2</sub>O<sub>3</sub> system.

We also refine the  $P$ - $V$ - $T$  equation of state of Al-bearing seifertite based on volume measurements up to more than 160 GPa and 4000 K [ $V_0 = 92.73(10) \text{ \AA}^3$ ,  $K_0 = 304.2(3.0) \text{ GPa}$ ,  $K'_0 = 4.59$  (fixed),  $\Theta_{D0} = 1130 \text{ K}$  (fixed),  $\gamma_0 = 1.61(3)$ ]. At 300 K, the volume decrease at the CaCl<sub>2</sub> to  $\alpha$ -PbO<sub>2</sub> transition is 0.5(1)%, a value slightly lower than the 0.6% reported previously for Al-free samples. At high temperature, the Grüneisen parameter of seifertite is found to be similar to that of stishovite. Nevertheless, the  $\Delta V/V$  across the CaCl<sub>2</sub>-form to seifertite transition is found to increase slightly with increasing temperature.

Across the phase transition, volume changes can be translated into density changes only when the Al substitution mechanisms in both CaCl<sub>2</sub>-form and seifertite are defined. The analysis of all available data sets suggests different substitution mechanisms for the two SiO<sub>2</sub> polymorphs. Al-substitution could occur via O-vacancies in the CaCl<sub>2</sub>-form and via extra interstitial Al in seifertite. This would result in a density increase of 2.2(3)% at 300 K for SiO<sub>2</sub> in basaltic lithologies. Alternatively, the same Al-substitution mechanism in both of the SiO<sub>2</sub>-dominated phases would yield a density increase of 0.5(1)%.

**Keywords:** Seifertite, phase transition in SiO<sub>2</sub>,  $P$ - $V$ - $T$  equation of state, lowermost Earth mantle

### INTRODUCTION

Seismic tomography suggests that the slab behavior depends primarily on the original plate velocity, the penetration angle of the slab into the mantle and the age of the subducted crust. In several regions the slabs appear to flatten and be delayed near the 660 km discontinuity. In most regions, however, slabs eventually descend through the lower mantle (e.g., van der Hilst et al. 2007; van der Meer et al. 2010). The sinking of subducting slabs in the deep mantle is controlled primarily by the density difference between the slab materials and the ambient mantle, while the mantle viscosity governs the speed of the descent. Detailed tomographic mapping of high-velocity regions in the mantle and comparison with surface paleogeography indicate that most slab remnants sink through the entire mantle in about 250 Ma, i.e., with an average speed of about 1.2 cm/year (van

der Meer et al. 2010).

The slab density is partly related to the slab temperature but also to the intrinsic density of the various minerals and their relative proportions. Older and relatively colder slabs are expected to penetrate the deep mantle more easily. Still, a major complication is the layered structure of the subducted slab, including its sedimentary, basaltic, and harzburgitic components. The density inversion between peridotite and basaltic material in the uppermost 50–100 km of the lower mantle caused by gradual transformation of majoritic garnet (e.g., Ringwood 1991) led to the suggestion of partial segregation (flotation) of garnetite near the 660 km discontinuity. The low temperature and high viscosity of slab material, however, make such a lithological separation unlikely. Another possible site of basalt-peridotite separation is the core-mantle boundary (CMB) region. Sinking slab material deflected laterally along the CMB thermal boundary layer will be heated considerably, resulting in reduced viscosity (e.g., Steinberger and Calderwood 2006). Even moderate basalt-

\* E-mail: D.Andrault@opgc.univ-bpclermont.fr

peridotite density contrasts in the D'' zone could, therefore, lead to such separation.

Difference in chemical composition between basaltic and peridotitic materials yields largely different mineral assemblages and mineral compositions at deep mantle *P-T* conditions. Peridotites varying from fertile lherzolite to depleted harzburgite are dominated by Mg-perovskite (pv, 70–80%) with minor amounts of ferropericlasite (15–25%) and Ca-perovskite (Ca-pv, 0–10%). Basalts have 3–10 times higher concentrations of Al, Ti, Ca, and Na and more than 5 times lower concentration of Mg than peridotite. The resulting lower mantle basaltic mineralogy has no ferropericlasite and a low proportion of Mg-perovskite (or post-perovskite) with high Fe/Mg-ratio. Over-abundance of silica and alumina produces the separate silica-dominated (Irfune et al. 1994) and Al-rich phases (NAL and Ca-ferrite phases) (Akaogi et al. 1999; Miyajima et al. 1999). At intermediate lower mantle depths, common basalts crystallize 15–20% CaCl<sub>2</sub>-structured silica, 15–25% Ca-ferrite, 35–40% Mg-perovskite, and 20–30% Ca-perovskite (Hirose et al. 1999). It is generally estimated that the Fe-rich Mg-perovskite makes basaltic material denser than peridotite throughout the lower mantle below 720 km depth (e.g., Guignot and Andrault 2004; Hirose et al. 2005; Ricolleau et al. 2010). Partly due to its elevated bulk modulus, the CaCl<sub>2</sub>-structured silica phase becomes the least dense phase of the subducted slabs at 70–120 GPa, with a density difference of more than 3% relative to the most abundant Mg-rich silicate perovskite.

At ~2500 K, pure SiO<sub>2</sub> was reported to undergo a first-order phase transformation from the CaCl<sub>2</sub>-form to seifertite (adopting the  $\alpha$ -PbO<sub>2</sub>-structure, El Goresy et al. 2008) at ~120 GPa, with a *dp/dT*-slope of about 10 MPa/K (Murakami et al. 2003). In parallel, Hirose et al. (2005) showed that the silica-dominated phases in a basaltic composition display considerable Al<sub>2</sub>O<sub>3</sub> solubility. The presence of Al<sub>2</sub>O<sub>3</sub> produces a considerable pressure reduction of the stishovite to CaCl<sub>2</sub>-phase transition, from ~50 GPa for pure SiO<sub>2</sub> to ~25 GPa for Al-bearing silica (Bolfan-Casanova et al. 2009; Lakshtanov et al. 2007b). On the other hand, the effect of Al<sub>2</sub>O<sub>3</sub> on the CaCl<sub>2</sub>-form to seifertite transformation and on the density change associated with this transition remains poorly constrained. Our objective here is to further evaluate the phase and density relations in the binary silica-alumina system at the *P-T* conditions of the lowermost mantle.

## EXPERIMENTAL METHODS

Silica glasses with 4 and 6 wt% Al<sub>2</sub>O<sub>3</sub> were prepared in Pt-crucibles at 1650–1670 °C in air, using a vertical furnace at Centre for Material Science, University of Oslo, and a Nabertherm furnace at Bayerisches Geoinstitut, Bayreuth, Germany. Tiny air bubbles persisted even after 3–4 repetitions of re-grinding and re-melting. Electron probe microanalyses yield Al-contents of 4.1(4) and 5.8(3) for glasses Al-4% and Al-6%, respectively. Relatively high values of standard deviations denote persistence of some chemical heterogeneity in the glass. Our analytical precision yielded element totals of 99.7(2) and 99.5(2) for more than 20 measurements on glasses Al-4% and Al-6%, respectively. The glasses were finely powdered and mixed with 10–15 wt% Pt-powder, which served as a YAG laser absorber and a pressure indicator at high temperatures. Overall, our samples should be homogeneous on a 2–3  $\mu$ m scale, which corresponds to the size of our X-ray probe.

Pressures up to 120 GPa were generated by membrane-type diamond-anvil cells (DAC) equipped with beveled diamonds of 150/300 or 100/300  $\mu$ m diameters. Rhenium gaskets were pre-indented to ~25  $\mu$ m thickness before laser drilling or spark erosion of 40–60  $\mu$ m diameters holes. Sample pellets were loaded between two pieces of dry NaCl or KCl, which served as pressure-transmitting medium and thermal insulator from the diamonds. Temperatures up to more than 4000 K

were generated by two NIR ytterbium fiber lasers. The size of the hot spot on the sample was kept between 15 and 25  $\mu$ m by adjusting the distance between the focusing-lenses and the sample. Using the spectral radiometry method, precision in temperature determination is better than 50 K. This value is also a maximum for temperature fluctuations at high temperature. Because phase transformations between dense silica polymorphs are known to be sluggish and depend on the starting material and pressure–temperature history (Prakapenka et al. 2004), we heated for 20–40 min at each temperature point.

Pressures at 300 K were determined based on the equation of state (EoS) of platinum (Holmes et al. 1989). It enabled quantitative comparisons with previous reports on the formation of seifertite (mostly Hirose et al. 2005; Murakami et al. 2003), in which Pt (Holmes et al. 1989) or Au (Tsuchiya 2003) EoS was used. Pressures derived from Pt and Au were reported to be fully compatible between each other (Hirose et al. 2005). Alternatively, we used the NaCl-B2 EoS that was calibrated against Pt (Sata et al. 2002). NaCl provided accurate pressure measurements after annealing at low temperature, when the Pt diffraction peaks remain broad due to poor release of the deviatoric stresses in the silica glass. At high temperature, the Pt that was intimately mixed with the starting material was used as a reliable sample-pressure indicator. We observed that the pressures measured at high temperatures were consistent with a pressure correction  $\Delta P = 2.5 \times 10^{-3}$  GPa/K (Andrault et al. 1998) compared to the nominal pressure measured at 300 K. The pressure error was estimated to be about 3%.

Angle-dispersive X-ray diffraction was performed in situ at the P02.2 (PETRA III, DESY) and ID27 (ESRF) beamlines. We used a monochromatic X-ray beam tuned at 42.7 keV (P02.2) or 33 keV (ID27) focused to less than  $2 \times 2 \mu\text{m}^2$  FWHM by two mirrors in the Kirkpatrick-Baez configuration. Diffraction images were acquired on a Perkin Elmer flat panel (P02.2) or Mar-CCD (ID27) detector with exposure times of 10–30 s, with or without sample rotation. Distance between sample and detector of 451 mm (P02.2) or 223 mm (ID27) was calibrated using a CeO<sub>2</sub> (P02.2) or LaB<sub>6</sub> (ID27) standard. Diffraction patterns were integrated and treated using the Fit2D (Hammersley 1996) and the GSAS (Larson and Von Dreele 1988) codes (Figs. 1 and 2). The orthorhombic lattice (*Pbcn*) of seifertite contains 4 independent parameters for atomic positions plus thermal factors for Si and O atoms. Due to the limited number of crystallites present in the X-ray spot, we preferred to avoid refinement of all those parameters. We first performed full X-ray profile refinement, using the Rietveld mode and keeping all atomic positions fixed to the values previously reported in the literature [upper frames in Fig. 2 (El Goresy et al. 2008)]. Although the atomic parameters may evolve slightly with *P* and *T*, the changes will be minor because these parameters are closely linked to the atomic arrangement within the lattice. Consequently, the evolution of the diffraction peaks intensity with pressure should also be reduced. This technique allows to model the experimental peaks with *d<sub>hkl</sub>* lines of comparable intensities and prevents evolution of the orthorhombic lattice toward solutions that are favorable from a mathematical rather than physical point of view. In a second step, we verified the adequateness between all experimental and theoretical diffraction features, using the Le Bail mode in which the peak intensities are adjustable parameters [lower frames in Fig. 2 (Le Bail 1992)]. For the NaCl or KCl pressure medium and platinum, we adjusted each diffraction line intensity independently using the Le Bail method, to obtain a best refinement of the diffraction profile. More than 20 diffraction lines were used to identify the CaCl<sub>2</sub>-structure and seifertite in 2- $\theta$  ranges between 5 and 18 (P02.2) and 6 and 22 (ID27) degrees. The reduced  $\chi^2$  value are typically 0.15 or 0.07 for seifertite (or the CaCl<sub>2</sub>-form) refined in Rietveld or Le Bail modes, respectively. The error in volume determination is less than 0.3%. The XRD data were acquired repeatedly during heating and after quenching to room temperature.

## PHASE TRANSFORMATION FROM CaCl<sub>2</sub>-FORM TO SEIFERTITE

We conducted five different runs (4 at P02.2 and 1 at ID27) of stepwise compression at 300 K followed by laser heating at successively higher temperatures. When the same sample was used for repeated experiments at increasing pressure, previously unheated sample areas were investigated at each new pressure. Crystallization of the CaCl<sub>2</sub>-form from the silica glass was obtained after laser heating to 2500 K at 91, 98, and 106 GPa and at 90 and 107 GPa for the samples containing 4 and 6 wt% Al<sub>2</sub>O<sub>3</sub>, respectively. After further steps of incremental pressurization, heating led to the formation of seifertite at nominal pressures of 119 and 121 GPa in the samples with 4 and 6 wt% Al<sub>2</sub>O<sub>3</sub>, respec-

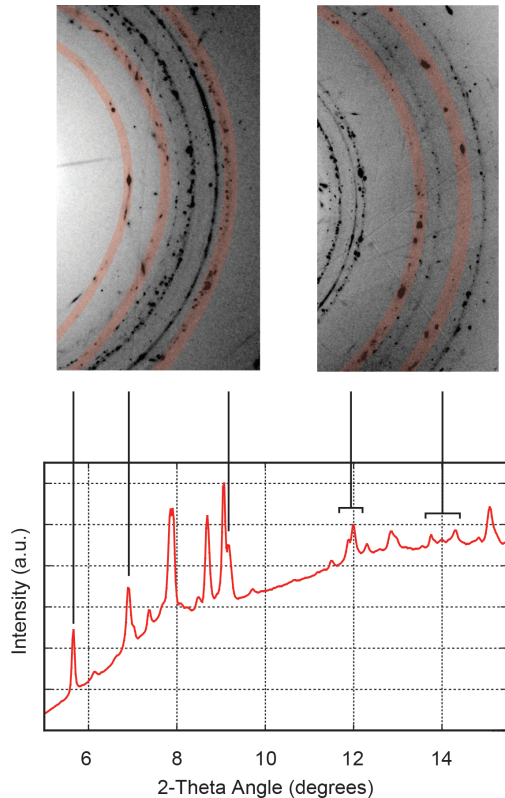


**FIGURE 1.** Selected regions of the 2D diffraction image (upper frames) and its spectral integration (lower frame) recorded in situ at 120 GPa and 2500 K. Regions where major seifertite diffraction peaks occur are colored in red. The number of seifertite crystallites is insufficient for a full structural refinement using the Rietveld method. However, the diffraction peak intensities are in good agreement with the structural model of seifertite (see Fig. 2). (Color online.)

tively. In the fifth experiment performed on the Al-6% glass at the ID27 beamline, we observed pure  $\text{CaCl}_2$ -phase up to 108 GPa and 2500 K, a mixture of the two silica polymorphs between 108 and 118 GPa, and pure seifertite starting from this pressure. Those results pinpoint at  $\sim 2500$  K the transition pressures at 108–119 and 108–118 GPa for Al-4% and Al-6% compositions, respectively. Those values are compatible with previous studies: At similar temperatures, the transition pressure was reported at 122 GPa for pure  $\text{SiO}_2$  (Murakami et al. 2003) and between 100 and 113 GPa for MORB compositions (Hirose et al. 2005). Because our starting material is a glass, we did not observe any metastable formation of seifertite at about 80 GPa as reported previously from cristobalite starting material (Dubrovinsky et al. 2001; Shieh et al. 2005). The glass crystallization is completed above  $\sim 3000$  K (Figs. 1–3). In all cases, no further phase transformation was observed upon heating after the glass crystallization. Although additional Al-bearing phases were not detected, we cannot rule out  $\text{Al}_2\text{O}_3$  saturation of the  $\text{CaCl}_2$ -structured and seifertite phases. Such saturation would imply that the  $\text{Al}_2\text{O}_3$ -content in  $\text{SiO}_2$ -dominated phases are lower than the 4 or 6 wt% of our starting materials. However,  $\text{Al}_2\text{O}_3$  saturation in our seifertite is unlikely, because seifertite crystallized from a natural basalt was previously reported with 12.8 wt%  $\text{Al}_2\text{O}_3$  (Hirose et al. 2005).

Based on the available data, we draw a tentative phase diagram for the Al-bearing  $\text{SiO}_2$  compositions as a function of pressure (Fig. 4). Due to the presence of Al-rich Ca-ferrite (near the  $\text{MgAl}_2\text{O}_4$ - $\text{NaAlSiO}_4$  join), the  $\text{Al}_2\text{O}_3$  activity in a MORB composition is expected to be high but lower than unity. Therefore, the  $\text{Al}_2\text{O}_3$ -contents of 3.4 and 12.6 wt% of the  $\text{CaCl}_2$ -phase and seifertite, respectively, reported by Hirose et al. (2005), provide lower bounds for the  $\text{Al}_2\text{O}_3$  solubility limit in silica. These values can hardly be used to calculate an Al partition coefficient between the two phases ( $K_{\text{Al}}^{\text{CaCl}_2/\text{Seifertite}}$ ), because the changes in mineralogy in their samples, between 60 and 113 GPa, is likely to affect the Al-activity significantly. On the other hand, the pressure of 113 GPa for their run no. 6 corresponds to a higher bound for the  $\text{CaCl}_2$ -form to seifertite phase transition in case of saturation in  $\text{Al}_2\text{O}_3$ . The results for our two compositions provide constraints on the position of the phase loop between the two minerals. The binary phase loop tends toward lower pressure with increasing Al-content. We draw straight lines for phase boundaries compatible with all data sets in the phase diagram (Fig. 4). By comparing the Al-contents in  $\text{CaCl}_2$ -phase and seifertite at a given pressure, we calculate a  $K_{\text{Al}}^{\text{CaCl}_2/\text{Seifertite}}$  value of  $\sim 0.55(5)$ . For this value, the phase transformation, for example an Al-bearing silica composition with 5 wt%  $\text{Al}_2\text{O}_3$ , would extend from  $\sim 112$  to  $\sim 116$  GPa, a pressure gap corresponding to a  $\sim 70$  km thick transition interval at a depth of  $\sim 2500$  km.

## RESULTS FOR THE $\text{CaCl}_2$ -FORM OF SILICA

We report our  $\text{SiO}_2$  volumes measured at 300 K for the  $\text{CaCl}_2$ -form below the transition pressure (Fig. 5a). We also report the data sets available for starting materials made of pure  $\text{SiO}_2$  (Andrault et al. 2003; Murakami et al. 2003), MORB (Hirose et al. 2005), and an Al-bearing  $\text{SiO}_2$  glass with 4 wt%  $\text{Al}_2\text{O}_3$  (Bolfan-Casanova et al. 2009). In the latest study, stishovite was synthesized with an estimated  $\text{Al}_2\text{O}_3$ -content of 2.2–3.6 wt%, for a starting material containing 4 wt%. This range of values is comparable to 3.4 wt%  $\text{Al}_2\text{O}_3$  measured in the  $\text{CaCl}_2$ -form by Hirose et al. (2005) and slightly less than the 4 and 6 wt%  $\text{Al}_2\text{O}_3$  present in our starting materials. At this point, it is interesting to note significant differences in the  $\text{CaCl}_2$ -form volumes between previous studies. The lowest compression curve, by  $\sim 1\%$  of volume or 6 GPa compared to our previous studies, is that of pure  $\text{SiO}_2$  reported by Murakami et al. (2003). At mid-distance between those two curves plot the compression curve of MORB (Hirose et al. 2005). These differences could be due to a difference in pressure determination or in volume measurement of the silicate phase. Because no pressure medium was used in the previous studies, the most likely cause of experimental difference originates from pressure determination. The volume relaxation from high temperature to 300 K for metallic blobs of Pt or Au pressure markers enclosed in a hard silica matrix can be hampered when shutting down the IR-laser. However, the volume change at the transition from  $\text{CaCl}_2$ -form to seifertite should be precise and significant for all studies, because the same experimental procedure was used throughout.

Our data set plots in perfect agreement with our prior studies performed on Al-free (Andrault et al. 2003) and 4 wt%  $\text{Al}_2\text{O}_3$  (Bolfan-Casanova et al. 2009), irrespective of Al-composition. Using the same experimental methods, compression curves of the 4 starting materials (2 in previous studies and 2 in the present

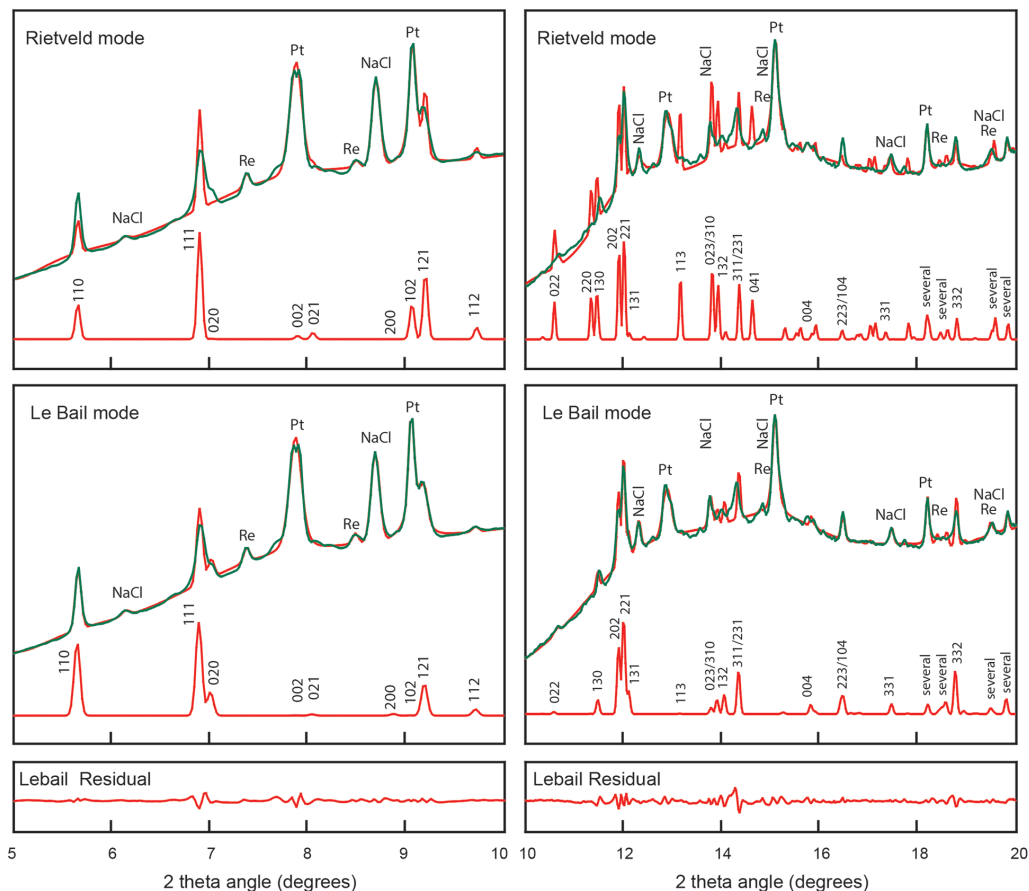


**FIGURE 2.** The diffraction spectra are refined in two steps. We first perform a full X-ray profile refinement, using the Rietveld mode and the structural model of seifertite (upper frames). Differences between experimental and calculated peak intensities are due to (1) change with pressure and temperature of the seifertite atomic parameters; the structural model that we used corresponds to ambient  $P$ - $T$  conditions (El Goresy et al. 2008), and (2) an insufficient number of crystallites in the X-ray spot. In a second step, we perform a profile refinement using the Le Bail mode (lower frames; see text). In each frame, green, upper red, and lower red spectra correspond to the experimental data, fully refined profile, and seifertite contribution, respectively. We also present the major  $d_{hkl}$  indexation of the seifertite diffraction peaks (we report “several” when more than two seifertite diffraction peaks plot at the same  $2\theta$  position). Left and right frames present the same experimental spectrum in  $2\theta$  ranges of 5–10 and 10–20°, respectively. (Color online.)

one) are found within the experimental error. It shows that Al presents a negligible effect on the volume of  $\text{CaCl}_2$ -structured silica at very high pressures. A study specifically dedicated to the effect of Al on the stishovite bulk modulus, using Brillouin scattering at ambient conditions, showed that addition of 6 wt%  $\text{Al}_2\text{O}_3$  induces a ~8% decrease in bulk modulus  $K_0$  (Lakshtanov et al. 2007a). However, the well-known tradeoff between  $K_0$ , its first pressure derivative  $K'_0$ , and maybe also second derivative  $K''_0$ , makes the compression curve very similar at high pressures. In our previous studies (dotted black line in Fig. 5a), the Birch-Murnaghan formalism was used to refine an isothermal (300 K) compression curve with the following parameters:  $V_0 = 46.77 \text{ \AA}^3$ ,  $K_0 = 292 \text{ GPa}$ , and  $K'_0 = 4.59$  (see sample PV-20 in Table 1 of Bolfan-Casanova et al. 2009), where  $V_0$  is the unit-cell volume at standard  $P$ - $T$  conditions. In this study, we preferred the use of the Vinet EoS formalism for reference isotherms, to facilitate the comparison with a recent study on stishovite (Wang et al. 2012). We therefore adjusted the previous compression curve using the

Vinet EoS and obtained  $V_0 = 46.77 \text{ \AA}^3$  (fixed),  $K_0 = 297(7) \text{ GPa}$ , and  $K'_0 = 4.59$  (fixed).

To our knowledge, there is no study reporting the EoS of the  $\text{CaCl}_2$ -form of Al-bearing  $\text{SiO}_2$  phases at high pressures and temperatures. A previous work performed up to 54 GPa and 1700 K reports the following parameters for the high temperature properties of stishovite:  $\Theta_{D0} = 1130 \text{ K}$ ,  $\gamma_0 = 1.67$ ,  $a = 1$ ,  $b = 3$ , where  $\Theta_{D0}$ ,  $\gamma_0$ , and  $a$  and  $b$  are the Debye temperature, the Grüneisen parameter at standard  $P$ - $T$  conditions, and two parameters for the change of Grüneisen parameter with volume, respectively (Wang et al. 2012). The EoS formalism was based on Mie-Grüneisen-Debye to model the high-temperature properties. In absence of a more reliable data set, we assume the following parameters to estimate volumes of the  $\text{CaCl}_2$ -form at all  $P$ - $T$  conditions:  $V_0 = 46.77 \text{ \AA}^3$ ,  $K_0 = 297 \text{ GPa}$ ,  $K'_0 = 4.59$ ,  $\Theta_{D0} = 1130 \text{ K}$ ,  $\gamma_0 = 1.67$ ,  $a = 1$ , and  $b = 3$ . Based on this  $PVT$  EoS, we calculate volumes of the  $\text{CaCl}_2$ -form at 300, 2000, and 4000 K in the pressure range investigated in this study (Fig. 5b).



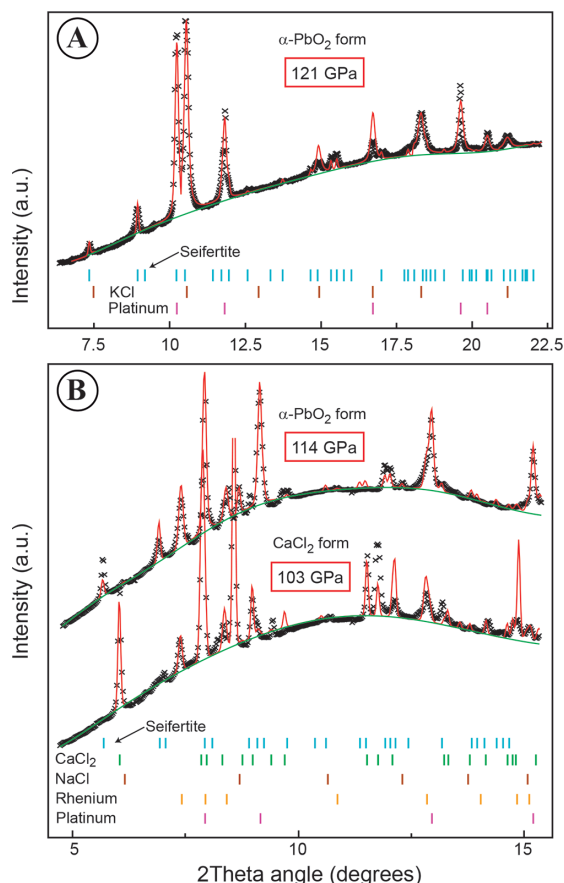


**FIGURE 3.** Examples of integrated X-ray diffraction patterns for the  $\text{CaCl}_2$ -structured silica phase and seifertite. These patterns were recorded (a) on ID-27 beamline at 3400 K and 121 GPa and (b) on P02.2 beamline after heating at 2500 K at 103 and 114 GPa. Small bumps on the diffraction patterns up to 2500 K are due to still incomplete transformation of the starting material. Platinum and the NaCl or KCl pressure medium are also visible. The reported pressure is based on the equation of state of Pt for the diffraction pattern recorded at high temperature before quenching. Black crosses, green lines, and red lines are experimental measurements, fitted background, and theoretical diffraction spectra, respectively. (Color online.)

### *P-V-T* equation of state of seifertite

We also report our  $\text{SiO}_2$  volumes measured at 300 K (Fig. 5a) and at temperatures up to 4300 K (Fig. 5b) for seifertite between the transition pressure and 162 GPa. Because seifertite and the  $\text{CaCl}_2$ -structured phase have 4 and 2 formula units per unit cell, respectively, we divide the seifertite volume by 2 to simplify the comparison. As for the  $\text{CaCl}_2$ -form, we also report data sets for pure  $\text{SiO}_2$  (Murakami et al. 2003) and MORB (Hirose et al. 2005). We first refine the *P-V*-300 K EoS of seifertite of Al-6 composition to  $V_0 = 92.73(10) \text{ \AA}^3$ ,  $K_0 = 304.2(3.0) \text{ GPa}$ , and  $K'_0 = 4.59$  (fixed), using the 14 data points recorded at ambient temperature in this study (Table 1). We fix  $K'_0$  because our experimental data set does not allow to adjust precisely the 3 parameters independently, due to the dependency between  $K_0$  and  $K'_0$  values. The seifertite bulk modulus appears very similar to that of the  $\text{CaCl}_2$ -form, only

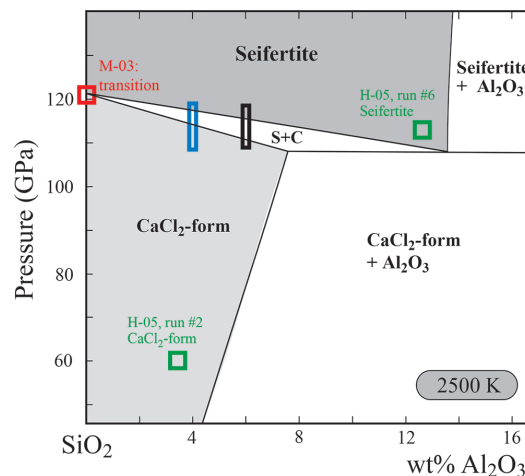


**FIGURE 4.** Approximate phase diagram for the  $\text{SiO}_2$ - $\text{Al}_2\text{O}_3$  system at 2500 K. For pure  $\text{SiO}_2$ , the phase transition is well defined at ~122 GPa (M-03; Murakami et al. 2003). For the mid-ocean ridge basalts used in H-05 (Hirose et al. 2005), the  $\text{CaCl}_2$ -form and seifertite phases were observed at 100 and 123 GPa, respectively. Concerning our samples, the rectangles represent the pressure range between our samples where  $\text{CaCl}_2$ -form or seifertite was synthesized. The pressure uncertainty of 3 GPa is included in the rectangle sizes. The loop diagram represented here is the widest model remaining compatible with the different data sets. (Color online.)

~2% higher than the value of 297 GPa recalculated for  $K'_0 = 4.59$ , based on a study using precisely the same experimental methods (Bolfan-Casanova et al. 2009). If we fix  $K'_0 = 5.0$ , we obtain  $V_0 = 93.75(10) \text{ \AA}^3$  and  $K_0 = 270.3(3.0) \text{ GPa}$ . The bulk modulus is found ~7% lower than the 292 GPa reported for stishovite in a previous study using a large volume press apparatus (Wang et al. 2012).

At high temperature, we refine  $\Theta_{D0} = 1130 \text{ K}$  (fixed),  $\gamma_0 = 1.61(3)$ ,  $a = 1$  (fixed), and  $b = 3$  (fixed) (Table 2), using the 16 data points recorded in this study (Table 1). The choice of fixing  $\Theta_{D0}$ ,  $a$ , and  $b$  is to facilitate the quantitative comparison with a previous study on stishovite (Wang et al. 2012). With these parameters, the maximum difference between the experimental and theoretical pressures is 2.7 GPa, which is within the experimental uncertainties. The refined room-pressure Grüneisen parameter of seifertite appears very similar to that proposed recently for stishovite, which was reported as 1.67 (Wang et al. 2012). In the *P-T* range investigated, we calculate Debye temperature and Grüneisen parameter mean values of  $\Theta_D = 1488(20) \text{ K}$  and  $\gamma = 0.78(4)$ , respectively (the  $\Theta_{D0}$  and  $\gamma_0$  reported above are ambient values). Based on this *P/T* EoS, we calculate volumes of seifertite at 300, 2000, and 4000 K for the pressure range investigated in this study (Fig. 5b).

We finally analyzed the evolution of the seifertite cell parameters with pressure (Fig. 6). We treated the fictive volumes  $a^3$ ,  $b^3$ , and  $c^3$  in a similar manner like seifertite unit-cell volumes. It results in a set of isothermal and high-temperature elastic parameters (Table 2). The Seifertite unit cell is quite anisotropic at high *P* and *T*, with the *a* parameter being 30% less incompressible than *b* and *c*, and with the *b* parameter showing a Grüneisen parameter about twice of *a* and *c*.

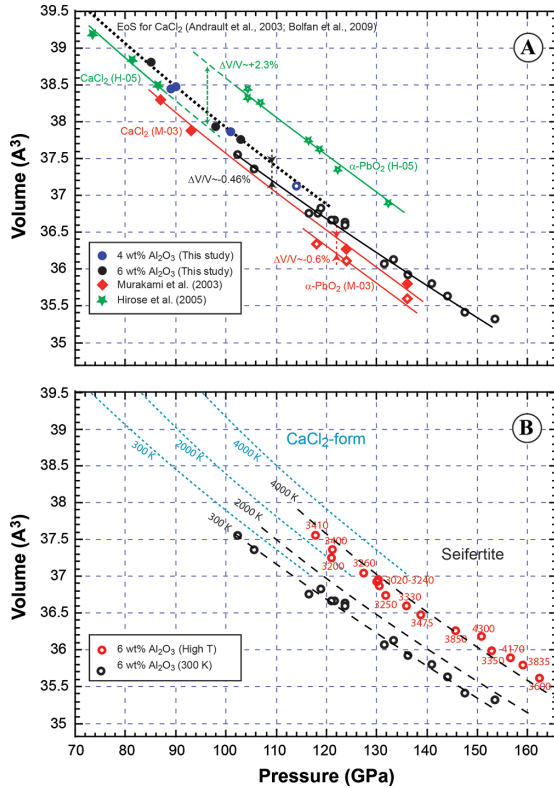


**FIGURE 5.** (a) Volumes of the two silica polymorphs measured around the transition pressure at 300 K. We also report the data sets reported for pure SiO<sub>2</sub> (red: Murakami et al. 2003; black dotted line: Andrault et al. 2003), a MORB-type material (green: Hirose et al. 2005), and an Al-bearing SiO<sub>2</sub> glass with 4 wt% Al<sub>2</sub>O<sub>3</sub> (black dotted line: Bolfan-Casanova et al. 2009). Closed and open symbols represent the CaCl<sub>2</sub>-phase and seifertite, respectively. (b) High-temperature volumes (red circles) recorded for seifertite from 100 to 162 GPa and up to 4300 K. We report the isothermal compression curves calculated at 300, 2000, and 3000 K for the CaCl<sub>2</sub>-form (blue dotted lines) and seifertite (dashed black lines) based on the *PVT* EoS refined in this study. (Color online.)

### Density change across the phase transition

A comparison between the 300 K isothermal compression curves of the CaCl<sub>2</sub>-form and seifertite of Al-6 composition evidences a volume change  $\Delta V/V = -0.5(1)\%$  across the phase transition (Fig. 5a). This value is very comparable to the volume changes of  $-0.6\%$  refined for pure SiO<sub>2</sub> (Murakami et al. 2003). For temperatures of 2000 and 4000 K, we refine volume changes of  $-0.52(10)\%$  and  $-0.62(10)\%$ , respectively, based on the *PVT* EoS (Fig. 5b). The fact that  $\Delta V/V$  increases slightly with temperature is compatible with a Grüneisen parameter lower in seifertite compared to the CaCl<sub>2</sub>-form.

The volume reduction of  $-0.6\%$  observed for pure SiO<sub>2</sub> (Murakami et al. 2003) translates directly in a  $+0.6\%$  density change at the transition. However, the relationship between volume and density is more complex for Al-bearing SiO<sub>2</sub> compounds. Three different mechanisms are possible for the Al<sub>2</sub>O<sub>3</sub> insertion in SiO<sub>2</sub> (Bromiley et al. 2006; Hirose et al. 1999): (1) formation of one oxygen vacancy per two Si<sup>4+</sup> substituted by Al<sup>3+</sup>; (2) addition of

**TABLE 1.** Unit-cell parameters of seifertite of 6 wt% composition recorded from 100 to 162 GPa and 300 to 4300 K

<i>T</i> (K)	<i>P</i> (K)	<i>a</i> (Å)	<i>b</i> (Å)	Seifertite <i>c</i> (Å)	<i>V</i> (Å <sup>3</sup> )	<i>V</i> /2 (Å <sup>3</sup> )
300	102.4	3.785	4.722	4.201	75.10	37.55
3410	117.8	3.778	4.736	4.197	75.10	37.55
300	105.7	3.767	4.723	4.198	74.69	37.35
3400	121.2	3.779	4.717	4.190	74.69	37.35
3200	121.0	3.768	4.718	4.191	74.50	37.25
300	118.9	3.755	4.676	4.194	73.64	36.82
3020	130.0	3.761	4.688	4.188	73.83	36.91
3260	127.4	3.764	4.693	4.193	74.07	37.03
300	116.5	3.753	4.681	4.185	73.52	36.76
300	120.9	3.747	4.688	4.172	73.30	36.65
300	121.5	3.743	4.686	4.179	73.30	36.65
3225	130.5	3.745	4.694	4.193	73.71	36.85
3240	130.3	3.746	4.713	4.183	73.86	36.93
300	123.5	3.738	4.690	4.177	73.22	36.61
3250	131.7	3.741	4.696	4.182	73.46	36.73
3475	138.8	3.730	4.689	4.170	72.93	36.46
3330	135.9	3.740	4.692	4.171	73.18	36.59
300	133.3	3.717	4.664	4.168	72.26	36.13
3850	145.7	3.736	4.667	4.158	72.50	36.25
300	131.5	3.721	4.660	4.160	72.14	36.07
4300	150.8	3.731	4.661	4.161	72.35	36.18
300	136.2	3.715	4.651	4.158	71.84	35.92
4170	156.6	3.723	4.663	4.134	71.77	35.89
3350	152.9	3.719	4.660	4.151	71.95	35.97
300	140.8	3.716	4.659	4.136	71.60	35.80
3835	159.0	3.712	4.659	4.139	71.58	35.79
300	144.1	3.709	4.653	4.130	71.27	35.64
3600	162.3	3.703	4.652	4.134	71.21	35.61
300	147.4	3.695	4.634	4.136	70.82	35.41
300	153.4	3.692	4.628	4.135	70.65	35.33

Notes: Pressure is derived from the *PVT*-EoS of platinum (Holmes et al. 1989) and temperature was determined by radiometric measurements. Uncertainties are 3% for pressures, 50 K for high temperatures,  $\sim 0.005$  Å for (*a*, *b*, *c*) cell parameters, and  $\sim 0.1$  Å<sup>3</sup> for unit cell volumes. *V*/2 is the seifertite volume divided by 2, to allow comparison with the CaCl<sub>2</sub>-form (see Fig. 5).

**TABLE 2.** Elastic parameters refined for seifertite, as well as for its three fictive *a*<sup>3</sup>, *b*<sup>3</sup>, *c*<sup>3</sup> volumes

	Volume	<i>a</i> <sup>3</sup>	<i>b</i> <sup>3</sup>	<i>c</i> <sup>3</sup>
<i>V</i> <sub>0</sub> (Å <sup>3</sup> )	92.73(10)	71.0(5)	129.8(3)	92.9(5)
<i>K</i> <sub>0</sub> (GPa)	304.2(3.0)	205(9)	310(4)	291(10)
<i>K</i> <sub>0</sub>	4.59 <sup>a</sup>	4.59 <sup>a</sup>	4.59 <sup>a</sup>	4.59 <sup>a</sup>
$\Theta_{D0}$ (K)	1130 <sup>b</sup>	1130 <sup>b</sup>	1130 <sup>b</sup>	1130 <sup>b</sup>
$\gamma_0$	1.61(3)	3.01(7)	5.96(20)	2.83(10)
<i>A</i>	1 <sup>b</sup>	1 <sup>b</sup>	1 <sup>b</sup>	1 <sup>b</sup>
<i>B</i>	3 <sup>b</sup>	3 <sup>b</sup>	3 <sup>b</sup>	3 <sup>b</sup>

Notes: We used the Vinet isothermal compression curves and the Mie-Grüneisen approach for modeling the effect of temperature.  $\Theta_{D0}$ ,  $\gamma_0$ , and *a* and *b* are the Debye temperature, the Grüneisen parameter at ambient conditions, and two parameters for the change of Grüneisen parameter with volume, respectively, according to the EoS formalism described elsewhere (Wang et al. 2012). Some parameters were fixed following the reports: <sup>a</sup> Bolfan-Casanova et al. (2009) and <sup>b</sup> Wang et al. (2012).

one extra-interstitial Al<sup>3+</sup> (i.e., a total of four Al<sup>3+</sup>) when three Si<sup>4+</sup> are replaced; and (3) a coupled (Al<sup>3+</sup>, H<sup>+</sup>) substitution in the presence of hydrogen. Also, one should keep in mind that different substitution mechanisms could still coexist in the same silica phase. Deriving density changes from volume changes at the phase transition requires assumptions on the predominant Al substitution mechanism in both the low- and high-pressure forms of SiO<sub>2</sub>. The reason is that the number of atoms per unit cell, and thus the corresponding atomic mass, is not the same for the three different Al-substitution mechanisms. Based on volume variations available for various Al-bearing compositions, we calculate density changes that should be expected at

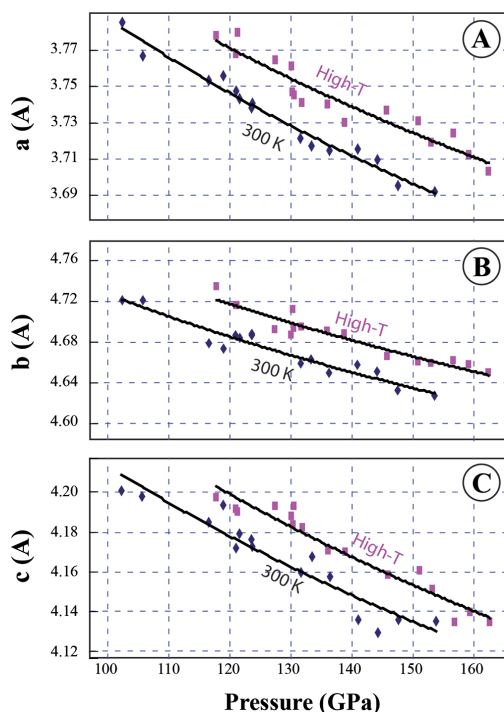


**FIGURE 6.** Seifertite (*a*, *b*, *c*) unit-cell parameters recorded at 300 K (blue diamonds) and up to 4300 K (purple rectangles) for pressures from 100 to 162 GPa. (Color online.)

the transition for all possible types of substitution mechanisms in  $\text{CaCl}_2$ -form and seifertite (Table 3).

Thermodynamic principles require a density increase (a positive  $\Delta\rho$ ) for the pressure-induced phase transformation irrespective of composition. Therefore, some Al-substitution mechanisms can be readily eliminated. First of all, having an identical substitution mechanism (ISM) for both polymorphs would yield a 2.3% density reduction at the transition pressure for Al-bearing silica in the MORB material (Hirose et al. 2005). This situation is not impossible, because this negative  $\Delta\rho$  could be counterbalanced by complementary mineralogical changes and element partitioning in the multi-component material. However, a largely negative  $\Delta\rho$  would be surprising and we therefore search for a more likely situation. The O-vacancy substitution mechanism in seifertite is unlikely, because this would cause negative  $\Delta\rho$  in our samples whatever is the  $\text{Al}_2\text{O}_3$ -substitution mechanisms in the  $\text{CaCl}_2$ -form (once the ISM case is discarded). In the same way, the Al-interstitial mechanism is unlikely in the  $\text{CaCl}_2$ -form. In a study at pressures up to 25 GPa, it was shown that the mechanism involving coupled  $\text{Al}^{3+}$  and  $\text{H}^+$  substitution can only explain 40% of the Al-substitution in stishovite (Litasov et al. 2007). In our experiments, particular care was taken to prevent the presence of water. Also, any water present in one polymorph is also likely to be present in the other, which would yield a similar Al-substitution mechanism in both polymorphs (the ISM case).

The most likely mechanisms are therefore the O-vacancy substitution in the  $\text{CaCl}_2$ -form and the  $\text{Al}^{3+}$ -interstitial substitution in seifertite (the OAI mechanism in Table 3). This is the only scenario in which the phase transition obeys the thermodynamic rule

**TABLE 3.** Measured volume changes ( $\Delta V/V$ ) and calculated density changes ( $\Delta\rho/\rho$ ) across the  $\text{CaCl}_2$ -form to seifertite transition (Fig. 5a)

	$\Delta V/V$ (%)	$\Delta\rho/\rho$ (%)						
		ISM	O→Al	Al→O	O→H	H→O	Al→H	H→Al
$\text{SiO}_2$ (M-03)	-0.60	0.60	0.60	0.60	0.60	0.60	0.60	0.60
Al-6 (This study)	-0.50	0.50	2.19	-1.16	1.56	-0.55	-0.12	1.12
MORB (H-05)	2.30	-2.30	0.23	-5.39	-1.72	-4.49	-3.23	-0.38

Notes: M-03 and H-05 stand for Murakami et al. (2003) and Hirose et al. (2005), respectively. The  $\Delta\rho/\rho$  are calculated using the measured  $\Delta V/V$ , taking into account all possible Al substitution mechanisms in  $\text{SiO}_2$  polymorphs. The  $\text{Al}^{3+}$  substitution can imply formation of an oxygen vacancy (O), insertion of extra-interstitial  $\text{Al}^{3+}$  (Al), or coupled  $\text{Al}^{3+}$ - $\text{H}^+$  substitution (H). The term "O→Al", for example, means a transition from an oxygen-deficient  $\text{CaCl}_2$ -form to a seifertite containing interstitial  $\text{Al}^{3+}$ . ISM = Identical substitution mechanism in both polymorphs.

of density increase for all the data sets available. It is compatible with a previous study showing that formation of O-vacancies is the predominant mechanism for the Al-substitution in stishovite (Bromiley et al. 2006). It remains unknown how it evolves with the increasing pressure in the rutile-structure, as well as across the structural distortion that yields the  $\text{CaCl}_2$ -type structure. For our samples with 4 or 6 wt%  $\text{Al}_2\text{O}_3$ , the O→Al mechanism would imply a ~2.19% density increase at the phase transition. This density increase is significantly larger than for the pure  $\text{SiO}_2$  system ( $\Delta\rho/\rho \sim 0.6\%$ ), in agreement with a lowering of the transition pressure with increasing the Al-content. In MORB, the density change is smaller, with a value of ~0.23%, because of the strong Al-partitioning into seifertite.

## IMPLICATIONS

Recent studies agree that basaltic materials of subducted slabs have a slight, but significant, density excess compared to a peridotitic lower mantle, even if the slabs are thermally equilibrated. Depending on composition and pressure, a density difference of 0.4 to 4.0 wt% was reported (Guignot and Andrault 2004; Hirose et al. 2005; Ono et al. 2005; Riccolleau et al. 2010). MORBs with elevated Fe-content are clearly denser. Despite the density excess, basaltic material under lower mantle conditions contains free silica phases, which are the lowest density phases at depths exceeding 1600–1800 km. Altogether, some studies suggest a decrease of the MORB density excess with increasing mantle depth (Guignot and Andrault 2004; Riccolleau et al. 2010) and others suggest a constant  $\Delta\rho$  (Hirose et al. 2005; Ono et al. 2005). For sedimentary material, the density is significantly lower than for MORB, due to low-Fe and high-Si contents (Guignot and Andrault 2004).

Our experimental results on compositions with 4–6 wt%  $\text{Al}_2\text{O}_3$  suggest a ~2.19% density increase for the transition from the  $\text{CaCl}_2$ -structured form to seifertite at 113–119 GPa and 300 K. At temperatures above 2000 K, this value should reach ~3%, due to higher volume change found for this transition at high temperature. The strong Al-partitioning from the  $\text{CaCl}_2$ -structured phase into seifertite will lead to compositional and density adjustments of the other Al-bearing phases in basaltic lithologies, in addition to the density effects caused by the silica-dominated phase transition. In subducted slab material the silica-dominated phases can represent up to about 20 and 40 vol% of MORB and sedimentary components, respectively (Hirose et al. 1999; Irifune et al. 1994). The  $\text{CaCl}_2$ -structured phase to seifertite transition could have a minor effect on the buoyancy in the peridotitic

mantle of the basaltic ocean crust of subducted slabs, because free-SiO<sub>2</sub> is not highly abundant and the MORB density is already significantly higher. For the sedimentary component, however, the CaCl<sub>2</sub> to seifertite transition may have a larger impact and facilitate the descent of the sedimentary material to the lowermost part of the mantle.

### ACKNOWLEDGMENTS

X-ray measurements were carried out at the light source PETRA III at DESY, a member of the Helmholtz Association (HGF), and at the ESRF. Experimental costs for the high-pressure experiments were defrayed by a Småforsk grant from the Research Council of Norway and the Programme National de Planétologie (INSU-CNRS). R.G.T. and W.M. are supported by CoE-grant 223272 (CEED) from RCN, and BMBF projects number 05K10RFA and 05K13RF1, respectively. We thank the *American Mineralogist* editors O. Tschauner and K. Putirka for their constructive work to improve this paper. This is a Clervolc contribution no. 99.

### REFERENCES CITED

- Akaogi, M., Hamada, Y., Suzuki, T., Kobayashi, M., and Okada, M. (1999) High pressure transitions in the system MgAl<sub>2</sub>O<sub>4</sub>-CaAl<sub>2</sub>O<sub>4</sub>: a new hexagonal aluminous phase with implication for the lower mantle. *Physics of the Earth and Planetary Interiors*, 115, 67–77.
- Andrault, D., Fiquet, G., Itié, J.P., Richet, P., Gillet, P., Häusermann, D., and Hanfland, M. (1998) Thermal pressure in a laser-heated diamond-anvil cell: An X-ray diffraction study. *European Journal of Mineralogy*, 10, 931–940.
- Andrault, D., Angel, R.J., Mosenfelder, J.L., and Le Bihan, T. (2003) Equation of state of the stishovite to lower mantle pressures. *American Mineralogist*, 88, 301–307.
- Bolfan-Casanova, N., Andrault, D., Amiguet, E., and Guignot, N. (2009) Equation of state and CaCl<sub>2</sub> transformation of Al-bearing stishovite up to 100 GPa and 3000 K. *Physics of the Earth and Planetary Interior*, 174, 70–77.
- Bromiley, G.D., Bromiley, F.A., and Bromiley, D.W. (2006) On the mechanisms for H and Al incorporation in stishovite. *Physics and Chemistry of Minerals*, 33, 613–621.
- Dubrovinsky, L.S., Dubrovinskaia, N.A., Saxena, S.K., Tutti, F., Rekh, S., Le Bihan, T., Shen, G.Y., and Hu, J. (2001) Pressure-induced transformations of cristobalite. *Chemical Physics Letters*, 333, 264–270.
- El Goresy, A., Dera, P., Sharp, T.G., Prewitt, C.T., Chen, M., Dubrovinsky, L., Wopenka, B., Boctor, N.Z., and Hemley, R.J. (2008) Seifertite, a dense orthorhombic polymorph of silica from the Martian meteorites Shergotty and Zagami. *European Journal of Mineralogy*, 20, 523–528.
- Guignot, N., and Andrault, D. (2004) Equations of state of Na-K-Al host phases in the lower mantle and implications for MORB density in the lower mantle. *Physics of the Earth and Planetary Interiors*, 134–144, 107–128.
- Hammersley, J. (1996) Fit2d user manual. ESRF, Grenoble, France.
- Hirose, K., Fei, Y.W., Ma, Y.Z., and Mao, H.K. (1999) The fate of subducted basaltic crust in the Earth's lower mantle. *Nature*, 397, 53–56.
- Hirose, K., Takafuji, N., Sata, N., and Ohishi, Y. (2005) Phase transition and density of subducted MORB crust in the lower mantle. *Earth and Planetary Science Letters*, 237, 239–251.
- Holmes, N.C., Moriarty, J.A., Gathers, G.R., and Nellis, W.J. (1989) Equations of state of platinum to 660 GPa (6.6 Mbar). *Journal of Applied Physics*, 66, 2962–2967.
- Irfune, T., Ringwood, A.E., and Hiberson, W.O. (1994) Subduction of continental crust and terrigenous and pelagic sediments: an experimental study. *Earth and Planetary Science Letters*, 126, 351–368.
- Lakshmanov, D.L., Litasov, K.D., Sinogeikin, S.V., Hellwig, H., Li, J., Ohtani, E., and Bass, J.D. (2007a) Effect of Al<sup>3+</sup> and H<sup>+</sup> on the elastic properties of stishovite. *American Mineralogist*, 92, 1026–1030.
- Lakshmanov, D.L., Sinogeikin, S.V., Litasov, K.D., Prakapenka, V.B., Hellwig, H., Wang, J.Y., Sanches-Valle, C., Perrillat, J.P., Chen, B., Somayazulu, M., Li, J., Ohtani, E., and Bass, J.D. (2007b) The post-stishovite phase transition in hydrous alumina-bearing SiO<sub>2</sub> in the lower mantle of the earth. *Proceedings of the National Academy of Sciences*, 104, 13588–13590.
- Larson, A.C., and Von Dreele, R.B. (1988) GSAS Manual. Report LAUR 86-748. Los Alamos National Laboratory.
- Le Bail, A. (1992) Extracting structure factors from powder diffraction data by iterating full pattern profile fitting. In E. Prince, and J.K. Stalick, Eds., *Accuracy in Powder Diffraction*, p. 213. National Institute of Standards and Technology (NIST), U.S.A.
- Litasov, K.D., Kagi, H., Shatskly, A., Ohtani, E., Lakshmanov, D.L., Bass, J.D., and Ito, E. (2007) High hydrogen solubility in Al-rich stishovite and water transport in the lower mantle. *Earth and Planetary Science Letters*, 262, 620–634.
- Miyajima, N., Fujino, K., Funamori, N., Kondo, T., and Yagi, T. (1999) Garnet-perovskite transformation under conditions of the Earth's lower mantle: an analytical transmission electron microscopy study. *Physics of the Earth and Planetary Interiors*, 116, 117–131.
- Murakami, M., Hirose, K., Ono, S., and Ohishi, Y. (2003) Stability of CaCl<sub>2</sub>-type and alpha-PbO<sub>2</sub>-type SiO<sub>2</sub> at high pressure and temperature determined by in-situ X-ray measurements. *Geophysical Research Letters*, 30, 1207.
- Ono, S., Ohishi, Y., Isshiki, M., and Watanuki, T. (2005) In situ X-ray observations of phase assemblages in peridotite and basalt compositions at lower mantle conditions: Implications for density of subducted oceanic plate. *Journal of Geophysical Research-Solid Earth*, 110, B02208.
- Prakapenka, V.P., Shen, G.Y., Dubrovinsky, L.S., Rivers, M.L., and Sutton, S.R. (2004) High pressure induced phase transformation of SiO<sub>2</sub> and GeO<sub>2</sub>: difference and similarity. *Journal of Physics and Chemistry of Solids*, 65, 1537–1545.
- Ricolleau, A., Perrillat, J.-P., Fiquet, G., Daniel, I., Matas, J., Addad, A., Menguy, N., Cardon, H., Mezouar, M., and Guignot, N. (2010) Phase relations and equation of state of a natural MORB: Implications for the density profile of subducted oceanic crust in the Earth's lower mantle. *Journal of Geophysical Research-Solid Earth*, 115, B08202.
- Ringwood, A.E. (1991) Phase-transformations and their bearing on the constitution and dynamics of the mantle. *Geochimica et Cosmochimica Acta*, 55, 2083–2110.
- Sata, N., Shen, G., Rivers, M.L., and Sutton, S.R. (2002) Pressure-volume equation of state of the high-pressure B2 phase of NaCl. *Physical Review B*, 65, 114114.
- Shieh, S.R., Duffy, T.S., and Shen, G.Y. (2005) X-ray diffraction study of phase stability in SiO<sub>2</sub> at deep mantle conditions. *Earth and Planetary Science Letters*, 235, 273–282.
- Steinberger, B., and Calderwood, A.R. (2006) Models of large-scale viscous flow in the Earth's mantle with constraints from mineral physics and surface observations. *Geophysical Journal International*, 167, 1461–1481.
- Tsuchiya, T. (2003) First-principles prediction of the P-V-T equation of state of gold and the 660-km discontinuity in Earth's mantle. *Journal of Geophysical Research-Solid Earth*, 108, 2462.
- van der Hilst, R.D., de Hoop, M.V., Wang, P., Shim, S.H., Ma, P., and Tenorio, L. (2007) Seismostratigraphy and thermal structure of Earth's core-mantle boundary region. *Science*, 315, 1813–1817.
- van der Meer, D.G., Spakman, W., van Hinsbergen, D.J.J., Amaru, M.L., and Torsvik, T.H. (2010) Towards absolute plate motions constrained by lower-mantle slab remnants. *Nature Geoscience*, 3, 36–40.
- Wang, F.L., Tange, Y., Irfune, T., and Funakoshi, K. (2012) P-V-T equation of state of stishovite up to mid-lower mantle conditions. *Journal of Geophysical Research-Solid Earth*, 117, B06209.

MANUSCRIPT RECEIVED JULY 29, 2013

MANUSCRIPT ACCEPTED APRIL 24, 2014

MANUSCRIPT HANDLED BY OLIVER TSCHAUNER